Draft version March 2, 2001
Preprint typeset using LaTeX style emulateapj v. 20/04/00

NEW TEMPERATURES OF DIFFUSE INTERSTELLAR GAS: THERMALLY UNSTABLE GAS

Carl Heiles
Astronomy Department, University of California, Berkeley, CA 94720-3411
Draft version March 2, 2001

ABSTRACT

We present new Arecibo 21-cm line measurements of the temperatures of interstellar gas. Our temperatures for the Cold Neutral Medium (CNM) are significantly lower than previous single-dish results and in very good accord with theoretical models. For warm gas at $T > 500$ K, we find a significant fraction of gas ($> 47\%$) to lie in the thermally unstable region $500 \rightarrow 5000$ K; moreover, about 60% of all the neutral atomic gas has $T > 500$ K. Large amounts of thermally unstable gas are not allowed in theoretical models of the global interstellar medium.

Subject headings: ISM:atoms—ISM:general—radio lines: ISM

1. INTRODUCTION

In 1977 McKee & Ostriker (MO) extended the two-phase model of Field, Goldsmith, & Habing (1969) by including supernovae (SN). Their interstellar medium (ISM) has four phases, if one includes the Warm Ionized Medium, and is dominated by individual SN explosions. The Hot Ionized Medium (HIM) fills the interior of SN remnants and powers their blast waves, which sweep up the gas inside the bubbles and pile it into the shells. Soon this shocked gas starts to cool and recombine rapidly, forming the Cold Neutral Medium (CNM). Soft X-rays produced by adjacent HIM penetrate the outsides of CNM clouds, heating the gas to form the Warm Neutral Medium (WNM).

The swept-up gas consists of two distinct neutral phases in physical contact, each in thermally stable equilibrium with equal thermal pressures. It is difficult to study such gas in individual SN remnants, but for superbubbles the general picture of hot gas inside a swept-out volume surrounded by dense walls is well corroborated by modern multiwavelength studies, for example in Eridanus (Heiles, Haffner, & Reynolds 1999).

Theoretical CNM and WNM temperatures are derived by calculating the equilibrium temperature as a function of thermal pressure. There exist two stable ranges of equilibrium, the CNM and the WNM with temperatures ~ 50 and ~ 8000 K, separated by a region of unstable temperatures (Wolfire et al 1995; WHMTB). Stable thermal pressure equilibrium, and thermal pressure equality between the phases, is a cornerstone of the MO theory.

Observational temperatures are derived in different ways for the CNM and WNM. For the CNM, the most accurate temperatures come from comparing 21-cm line absorption and emission profiles. The line opacity $\propto \frac{1}{T}$; only the CNM produces significant absorption lines, while the CNM and WNM both contribute to emission. In contrast, most WNM temperatures are derived from linewidths. 21-cm linewidths provide upper limits to temperature, while in some cases combining them with heavy element linewidths from optical/UV spectra provides actual temperatures (see review by Heiles 2000).

Kulkarni & Heiles (1987; KH) summarized temperature measurements of the CNM and WNM, confining their analysis to 21-cm line absorption/emission measurements because very few UV data were available at that time. For the CNM, they discussed single-dish results in terms of the conventional interpretation of clouds within which the temperature increases outwards. As briefly discussed below, each derived temperature is the lowest one in its cloud. Expressed as histograms, these coldest-cloud derived temperatures are broadly distributed over the range $20 \rightarrow 300$ K (Mebold et al 1982, MWKG; Dickey, Salpeter, & Terzian 1978, DST; Payne, Salpeter, & Terzian 1982, PST). In addition, there is a weakly significant statistical relationship between the derived CNM temperature and the 21-cm line opacity, called the $T - \tau$ relation. For the WNM, KH found that the limited data supported a lower limit ~ 5000 K, but they cautioned that the result needed confirmation.

In contrast, interferometric maps of a field around 3C147 (Kalberla, Schwarz, & Goss 1985, KSG) provide a completely different picture. For the CNM, the components are roughly isothermal and have colder temperatures ($34 \rightarrow 74$ K). For the WNM, which contributes $\sim 80\%$ of the mass, temperatures lie in the thermally unstable range ($500 \rightarrow 2000$ K). The high angular resolution should make these results reliable. However, such results are available in only a few fields. The fact that they conflict with the single-dish results is disturbing. The single-dish results are the ones always quoted in reviews because of their much larger statistical sample for the CNM; it is worth noting, though, that for the WNM the single-dish sample is no larger than the interferometric one.

Here we present a statistical summary of new single-dish temperatures. For the CNM they are derived from HI absorption/emission line data; for the WNM they are upper limits based on linewidths. We introduce a new analysis technique for absorption/emission observations. Our results are consistent with the 3C147 results. For the CNM, we find lower temperatures than previous single-dish workers; these are more in line with theoretical prediction for the CNM. For the WNM we find that most of the gas WNM is at thermally unstable temperatures; this disagrees with the MO theory.

2. NEW 21-CM LINE OBSERVATIONS

2.1. *Observations and reduction technique*

Heiles and Troland (2001) are performing a survey of Zeeman splitting of HI absorption lines with the Arecibo telescope[1]. These data have long integration times, which produces excellent signal/noise and makes them unsurpassed for obtaining temperatures. Our results are more accurate and cover more sources than the best previous surveys, which are the Arecibo work by DST[2] and PST, and the Bonn/NRAO work by MWKG. Here we report on 24 sightlines, 19 of which have $|b| > 20°$ but otherwise are randomly selected within Arecibo's declination range $\sim 0° \rightarrow 39°$.

Each absorption spectrum consists of very obvious velocity components and we represent their optical depths by a set of N Gaussians. Thus we least squares fit the observed spectrum $\frac{T_{abs}}{T_C} = e^{-\tau}$, where

$$\tau = \Sigma_0^{N-1} \tau_{0n} e^{-[(V-V_{0n})/\delta V_n]^2} \; ; \tag{1}$$

here $\frac{T_{abs}}{T_C}$ is the absorption profile divided by the continuum source strength and $(V_{0n}, \delta V_n)$ are (central velocity, $\frac{1}{e}$ width) of component n. We assume that each component is an independent physical entity, and is *isothermal*. This is consistent with the findings of KSG.

Each HI emission spectrum contains structure but, also, is wider than its associated absorption spectrum, as is well known. We assume that the emission spectrum $T_{em} = T_{CNM} + T_{WNM}$, where T_{CNM} is the contribution from the aforementioned CNM components. T_{WNM} is the contribution from K additional wide Gaussians to represent the WNM; K is small number and often just one. The spin temperatures in these additional components are so high that they have negligible optical depth and produce no easily discernible features in the absorption spectrum.

In least-squares fitting the emission, we include the absorption of more distant CNM Gaussians by less distant ones. Letting T_n be the spin temperature of component n, which is also the kinetic temperature,

$$T_{CNM} = \Sigma_0^{N-1} T_n (1 - e^{-\tau_n}) e^{-\Sigma_0^{M-1} \tau_m} \; , \tag{2}$$

where the subscript m with its associated optical depth profile τ_m represents each of the M CNM clouds that lie in front of cloud n. For multiple absorption components, we experiment with all possible orders along the line of sight and choose the one that yields the smallest residuals. We also include the absorption of each WNM component by the CNM by assuming that a fraction $\mathcal{F}_k$ lies in front of all the CNM and is unabsorbed, with the rest all lying behind; thus

$$T_{WNM} = \Sigma_0^{K-1} [\mathcal{F}_k + (1-\mathcal{F}_k) e^{-\tau}] T_{0k} e^{-[(V-V_{0k}/\delta V_k]^2} \; , \tag{3}$$

where the subscript k represents each WNM component. Note that T_{0k} is a brightness temperature, not a kinetic temperature. In most cases $\mathcal{F}_k$ is indeterminant and we can only distinguish between the two extremes $\mathcal{F}_k = (0, 1)$. The differences for different orderings are sometimes not statistically significant but nevertheless lead to differences in the derived CNM temperatures. These differences reflect the uncertainties in T_n more than the conventional errors derived from least squares fits. Additional uncertainties can occur if there are unresolved subcomponents. We defer discussion of these details to the more comprehensive paper (Heiles and Troland 2001).

Previous single-dish authors, in contrast, implicitly assume that clouds are *not* isothermal. They derive the spin temperature of a cloud at the peak of its absorption profile. Thus each point on their histograms represents the lowest derived temperature for that particular cloud. This temperature, however, is not the coldest temperature in the cloud, because the line of sight also passes through warmer gas.

2.2. *Sample result: 3C18*

Figure 1 exhibits the results for 3C18 [located at $(\ell, b) = (119°, -53°)$], which is a simple profile and good for an illustrative example. In the top panel the solid line is the observed absorption spectrum $\frac{T_{abs}}{T_C}$, which we fit with the three CNM components whose depths and halfwidths are indicated; the dash-dot line is the fit. In the bottom panel the solid line is the observed emission spectrum T_{em}. The dashed curve is T_{CNM}; the dotted is T_{WNM} fit with $K = 1$, which is unabsorbed by the CNM because the lowest residuals are obtained with $\mathcal{F} = 1$. The full fitted curve is the sum, shown as dash-dot, which is a good fit except in the extreme line wings where stray radiation makes the data suspect (e.g. Hartmann & Burton 1997).

For 3C18, the WNM component has halfwidth 10.0 km s^{-1}, which corresponds to purely thermal broadening at $T = 2200$ K; this is an upper limit on the kinetic temperature T_K. For the three CNM components, left-to-right on Figure 1, the halfwidths are $(2.5 \pm 0.03, 6.3 \pm 0.07, 1.1 \pm 0.15)$ km s^{-1} and spin temperatures are 32 ± 1, 43 ± 6, and 46 ± 9 K. The ratios of total linewidth to thermal linewidth are $(2.04 \pm 0.07, 4.50 \pm 0.63, 0.75 \pm 0.18)$; the 1σ uncertainty on the last ratio is statistically consistent with a ratio ≥ 1, as it must be. The (WNM, CNM) components contribute $N(HI) = (3.2, 1.8) \times 10^{20}$ cm^{-2}, respectively. The WNM/CNM ratio is ~ 1.8, which is close to our global average.

2.3. *Our ensemble of WNM temperatures*

Our 49 WNM components have linewidths that correspond to upper limits on the kinetic temperature. The top two panels of Figure 2 exhibit histograms of these limits, one for number of components and one for column density. Not included on these histograms is one absorption component for which the spin temperature was derived: $T_{spin} = 725$ K, $N(HI) = 1.4 \times 10^{20}$ cm^{-2}. Including this, 20 of the WNM components (40%) have $T_K = 500 \rightarrow 5000$ K. These contain $> 47\%$ of the total WNM column density; this is a lower limit because the WNM temperatures are upper limits. Because these components are not visible in absorption, their spin temperatures exceed ~ 500 K. This range, $500 \rightarrow 5000$ K, is approximately the thermally unstable range that separates CNM from WNM.

[1]The Arecibo Observatory is part of the National Astronomy and Ionosphere Center, which is operated by Cornell University under a cooperative agreement with the National Science Foundation.

[2]We find about half the DST absorption profiles to exhibit large differences from ours, with DST components being wider and multiply-peaked; some of DST's profiles were corrupted by local oscillator stability problems (Dickey, private communication). This completely explains the disagreement of Greisen and Liszt (1986) with DST for 3C348.

2.4. *Our ensemble of CNM temperatures*

Our 86 CNM temperatures are derived from absorption/emission data and are values, not upper or lower limits. The bottom two panels of Figure 2 exhibit histograms of these temperatures. The two histograms exhibit broad peaks in the range $T = 25 \rightarrow 75$ K. 47 of the CNM components (54%) have temperatures in this range; these contain 61% of the total CNM column density. We also see colder gas: 10 components (11%) containing 5% of the mass have $T = 10 \rightarrow 25$ K. We discount the four small-$N(HI)$ components having $T < 10$ K: they are weak and the temperatures have large errors. We find no support for the weakly significant $T - \tau$ relation reviewed by KH.

2.5. *Ratio of CNM and WNM components and mass*

For WNM gas ($T > 500$ K), we found 49 components with total $N(HI) = 107 \times 10^{20}$ cm^{-2}. For CNM gas ($T < 200$ K) we found 80 components having a total $N(HI) = 65 \times 10^{20}$ cm^{-2}. In the mildly ambiguous range $T = 200 \rightarrow 500$ K we found 6 components with total $N(HI) = 7.5 \times 10^{20}$ cm^{-2}. Thus, the ratio of CNM to WNM is, in terms of number of components, 1.6; in terms of mass, 0.60. Overall, our results indicate that about 60% of all the neutral atomic ISM is WNM, with $T > 500$ K.

2.6. *Temperatures from optical/UV absorption line observations*

To derive kinetic temperatures from an atomic optical/UV absorption line, one decomposes it into Gaussian components. Then one does the same with the 21-cm emission line toward the star, fixing the central velocities to be the same. The comparison of line widths separates the thermal and turbulent broadening. The derived temperatures are upper limits because the HI line comes from a much larger angular area so the nonthermal component of its width may be larger than that of the heavy element lines. Such temperatures are probably the best one can do for the WNM, but for CNM gas they are much less accurate than those derived from 21-cm absorption/emission line data.

Spitzer & Fitzpatrick (1995) and Fitzpatrick & Spitzer (1997) use this technique towards two high-latitude stars and derive temperatures and column densities for 21 diffuse neutral components. Of this total, 3 components have $T > 5000$ K, 13 have $T < 500$ K, and 5 have T in the unstable $500 \rightarrow 5000$ K range; thus, 24% of the components are thermally unstable; these contain 63% of the mass.

One can derive excitation temperatures of the low-J states of H_2 using UV absorption lines (Shull et al 2000; Spitzer, Cochran, & Hirshfeld 1974). These tend to agree with previous 21-cm line temperatures and are systematically higher than ours. If our temperatures are correct, then the low-J states are nonthermally populated, as are the high-J ones.

3. DISCUSSION AND COMPARISON WITH THEORY

3.1. *The WNM*

Both our new HI and the optical/UV observations show that much of the WNM—at least 47%—lies at temperatures that are unstable to isobaric perturbations. Our Arecibo data show this departure from thermal stability in a statistically convincing manner. Previous 21-cm line studies have hinted at this result. In emission/absorption studies, MWKG decomposed emission line profiles into Gaussians, with similar results; however, they didn't explicitly point out this departure. Verschuur & Magnani (1994) and Heiles (1989) analyzed emission profiles and found numerous components with widths in this range, but without absorption data could not conclusively state that the kinetic temperatures were indeed so high.

The large fraction of WNM in the thermally unstable regime violates a fundamental cornerstone of equilibrium ISM models such as MO, which all rely on thermal pressure equilibrium to push the gas into one of the thermally stable CNM or WNM phases. This result seems to push us towards other types of model. Two possibilities include time-dependent models such as the supernova-dominant model of Gerola, Kafatos, and McCray (1974) and turbulence-dominated models such as Vázquez-Semadeni, Gazol, & Scalo (2000).

3.2. *The CNM*

Figure 2 exhibits the histogram of derived spin temperatures for all CNM components. Both most of the components and most of the mass have $T = 25 \rightarrow 75$ K. This is in marked contrast to previous results, where histograms were broad over the ranges $20 \rightarrow 140$ K (MWKG) and $50 \rightarrow 300$ K (DST, PST). Our range is narrower and, moreover, temperatures extend to very low values, with significant contributions down to $T = 10$ K.

The peak above $T \sim 25$ K agrees very well with the high angular resolution results of KSG and, also, theory. WHMTB included all known processes in calculating their standard model, for which the CNM equilibrium temperatures range from $25 \rightarrow 200$ K (the corresponding densities are $n_{HI} \gtrsim 1000 \rightarrow 4$ cm^{-3}). Our observed temperature range is smaller and corresponds to $n_{HI} \gtrsim 250 \rightarrow 20$ cm^{-3} and $\frac{P}{k} = 10000 \rightarrow 1500$ cm^{-3} K. These numbers are in accord with ISM pressure measurements (Jenkins, Jura, & Lowenstein 1983).

Temperatures as low as our $10 \rightarrow 20$ K range can occur in the absence of the PAH-type grains that produce grain heating (WHMTB; Bakes and Tielens 1994). In this case, heating is by photoionization of Carbon and cooling by electron recombination onto ionized Carbon (Spitzer 1978). Such cold (and even colder) gas was invoked by Heiles (1997) to help understand the existence of tiny-scale atomic structure; the present results are encouraging for that interpretation.

It is a pleasure to acknowledge conversations with John Dickey, Alex Lazarian, Jeff Linsky, Chris McKee, Paolo Padoan, Tom Troland, Enrique Vázquez-Semadeni, and Ellen Zweibel. This work was partly supported by NSF grant AST9530590 to the author.

REFERENCES

Bakes, E.L.O. & Tielens, A.G.G.M 1994 ApJ, 427, 822.
Dickey, J.M., Salpeter, E.E., & Terzian, Y. 1978, ApJS, 36, 77 (DST).
Field, G.B., Goldsmith, D.W., & Habing, H.J. 1969, ApJ, 155, L149.
Fitzpatrick, E.L. & Spitzer, L. 1997, ApJ, 475, 623 (FS).
Gerola, H., Kafatos, M., & McCray, R. 1974, ApJ, 189, 55.
Greisen, E.W. & Liszt, H.S. 1986, ApJ, 303, 702.
Hartmann, Dap, and Burton, W.B. 1997, Atlas of Galactic Neutral Hydrogen, (Cambridge: Cambridge University Press).
Heiles, C. 1989, ApJ, 336, 808.
Heiles, C. 1997, ApJ, 481, 193.
Heiles, C. 2000, in Galactic Structure, Stars, and the Interstellar Medium (the Fourth Tetons Conference), ASP Conf Series 000, 000 (astro-ph/0010047).
Heiles, C., Haffner, L.M., & Reynolds, R.J. 1999 New Perspectives on the Interstellar Medium, Astronomical Society of the Pacific Conference Series 168, p 211.
Heiles, C. & Troland, T. 2001, ApJ, in preparation.
Jenkins, E.B., Jura, M., & Lowenstein, M. 1983, ApJ, 270, 88.
Kalberla, P.M.W., Schwarz, U.J., & Goss, W.M. 1985, A&A, 144, 27 (KSG).
Kulkarni, S.R. & Heiles, C. 1987, in Interstellar Processes, ed. D. J. Hollenbach & H.A. Thronson, Reidel, Dordrecht, p 87 (KH).
McKee, C.F. & Ostriker, J.P. 1977, ApJ, 218, 148 (MO).
Mebold, U., Winnberg, A., Kalberla, P.M.W., & Goss, W.M. 1982, A&A, 115, 223 (MWKG).
Payne, H.E., Salpeter, E.E., & Terzian, Y. 1982, ApJS, 48, 199 (PST).
Shull, J.M. et al 2000, ApJ, 538, L73.
Spitzer, L. 1978, Physical Processes in the Interstellar Medium, Wiley: New York, p. 143.
Spitzer, L., Jr., Cochran, W. D., & Hirshfeld, A. 1974, ApJS, 28, 373.
Spitzer, L. & Fitzpatrick, E.L. 1995, ApJ, 445, 196.
Vázquez-Semadeni, E., Gazol, A., & Scalo, J. 2000, ApJ, 540, 271.
Verschuur, G.L. & Magnani, L. 1994, AJ, 107, 287.
Wolfire, M.G., Hollenbach, D., McKee, C.F., Tielens, A.G.G.M., & Bakes, E.L.O. 1995a, ApJ, 443, 152 (WHMTB).

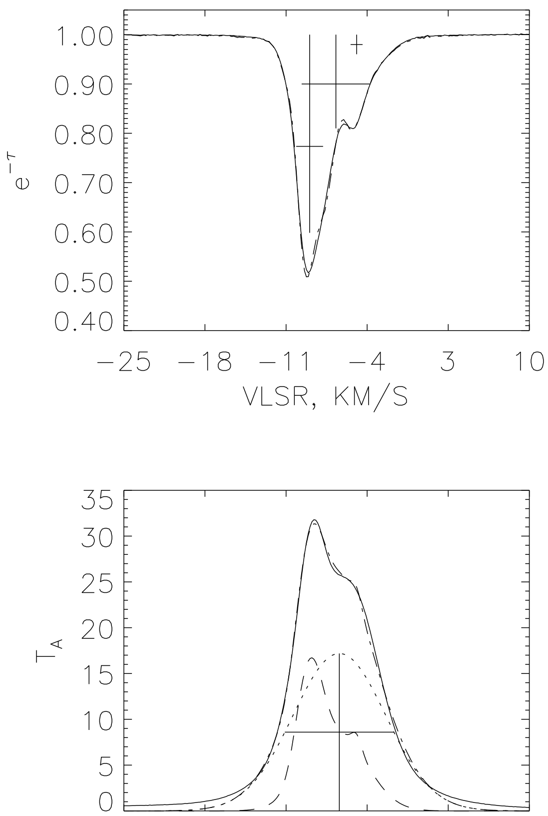

FIG. 1.— 21-cm line absorption (top) and emission (bottom) spectra for 3C18. In the absorption spectrum, the solid line is data and the dash-dot line the fit; crosses indicate the central $e^{-\tau}$'s and halfwidths of the three Gaussian component parameters. In the emission spectrum, the solid line is the data; the dashed line is the contribution from the three CNM components, the dotted line from the WNM component, and the dash-dot line their sum. Dash-dot lines in both figures are the fits and are so close to the data that they are hard to distinguish.

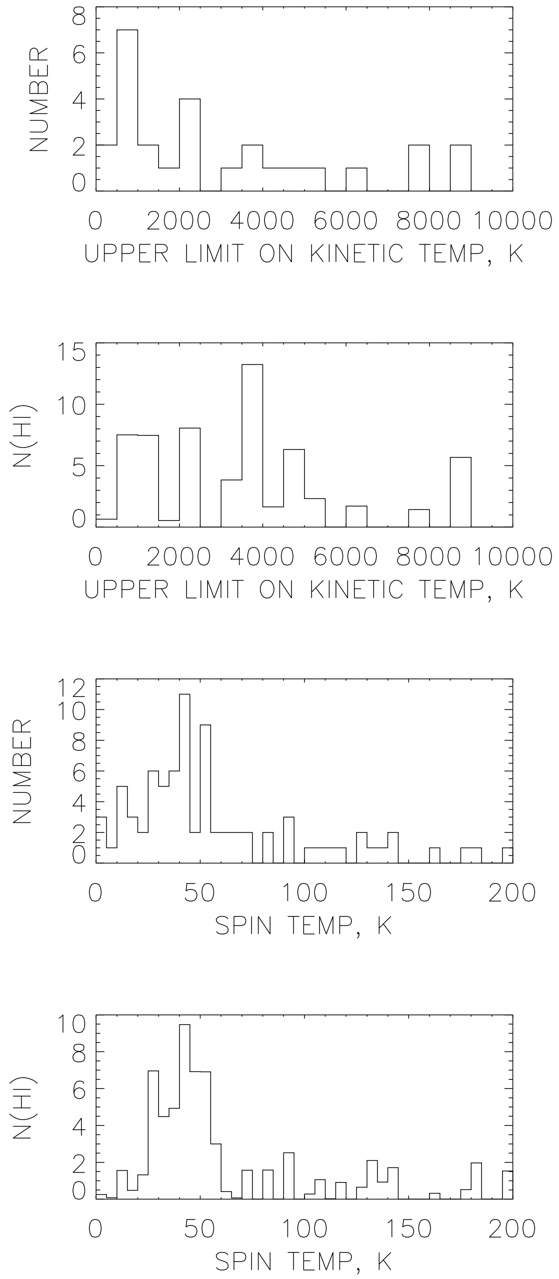

FIG. 2.— Histograms of derived temperatures. The top two frames are upper limits on kinetic temperature for the WNM derived from line widths; of these, the top gives the number of Gaussian components and the bottom the HI column density in units of 10^{20} cm^{-2}. Off the graphs to the right, with upper limits exceeding 10^4 K, are 21 components (44%) containing $N(HI)$ = 45 x 10^{20} cm^{-2} (43%). The bottom two frames are values (not limits) of spin temperature derived from absorption/emission data. Off the graphs to the right, with spin temperatures exceeding 200 K, are 8 components (9%)containing $N(HI)$ = 37 x 10^{20} cm^{-2} (36%).